

Real-Time Observation of CaCO_3 Mineralization in Highly Supersaturated Graphene Liquid Cells

Kyun Seong Dae, Joon Ha Chang, Kunmo Koo, Jungjae Park, Jae Sung Kim, and Jong Min Yuk*



Cite This: *ACS Omega* 2020, 5, 14619–14624



Read Online

ACCESS |



Metrics & More

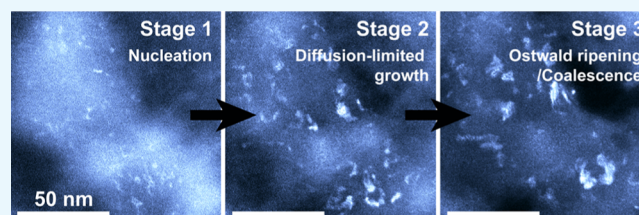


Article Recommendations



Supporting Information

ABSTRACT: The mineralization dynamics of calcium carbonate is investigated under highly supersaturated conditions using graphene liquid cell transmission electron microscopy. We demonstrate that the mineralization process has three steps: nucleation, diffusion-limited growth, and Ostwald ripening/coalescence. In addition, we show that the polymorphs precipitate in a specific order, from metastable aragonite to stable calcite, thus proving Ostwald's rule of stages. In highly supersaturated solutions, the aragonite phase crystallizes in a stable manner, in addition to the calcite phase.



1. INTRODUCTION

Calcium carbonate (CaCO_3), the principal component of limestone and marble, is one of the most abundant minerals in the earth.¹ The compound precipitates as sediment from the world's oceans,² speleothems (stalagmites, stalactites, etc.) in caverns,^{3,4} and unwanted deposits in plumbing and sewage systems.⁵ It also plays a significant role in the construction of marine organisms, including the shells of exoskeletons, the imaging eye lens of trilobites, and the love darts of gastropods.^{6,7} Calcium carbonate has a variety of polymorphs, including the three primary crystallographic phases of calcite, aragonite, and vaterite,⁸ which grow selectively according to the level of supersaturation.⁹ Because of academic and applied interest in the varying physical and chemical properties of these polymorphs, their mineralization has been studied extensively for decades using an X-ray diffractometer, Fourier-transform infrared spectroscopy (FT-IR), and thermogravimetry-differential thermal analysis (TG-DTA).^{10–15}

Even though *in situ* transmission electron microscopy (TEM) can provide direct imaging of polymorph precipitation, it has been rarely applied because precursor solutions are incompatible with the vacuum environment of the equipment. Recently, owing to the development of liquid cell TEM (LC-TEM), mineralization mechanisms previously unknown have been revealed at a restricted spatial resolution because of the electron-beam sensitivity of the minerals.^{16–19}

In this study, we used graphene liquid cell (GLC) TEM to investigate mineral precipitation under highly supersaturated conditions. The GLC is fabricated with a thin window of graphene separating the liquid specimen from the vacuum environment, which enables us to analyze the mineralization dynamics and the polymorphism evolution at an atomic level by direct *in situ* observation.

2. RESULTS AND DISCUSSION

Figure 1a shows a schematic of the GLC structure composed of graphene membranes and an entrapped reactant solution. We utilize multilayer graphene for both atomic resolution and high yield for GLC fabrication.²⁰ It is observed that the solution is successfully entrapped by the graphene membranes and extensively distributed throughout the TEM grid (Figure S1). Upon electron beam irradiation, the minerals are crystallized because of the evaporation of water and subsequent increase in supersaturation. Using high-resolution TEM (HRTEM), we identify the phases of the precipitates. Figure 1b shows the Wiener-filtered HRTEM images of the coprecipitated calcite and aragonite polymorphs in the GLC (raw images are shown in Figure S2). We confirm the phase of each particle by matching the HRTEM images with the simulated images. Remarkably, aragonite polymorphs, which are stable under highly supersaturated conditions, are newly formed during crystallization, in addition to calcite polymorphs. Although aragonite is more soluble than calcite, under high evaporation rates, the solution is supersaturated with aragonite.²¹

We track the mineralization dynamics with a series of dark-field TEM (DF-TEM) images (Figure 2a and Movie S1) acquired by selecting the diffraction spot of the precipitates (Figure S3). The thickness contrast of the solution gradually diminishes because of the evaporation of water. Gas products (H_2 , O_2 , and CO_2) are outgassed through the defects of the

Received: March 23, 2020

Accepted: May 29, 2020

Published: June 10, 2020



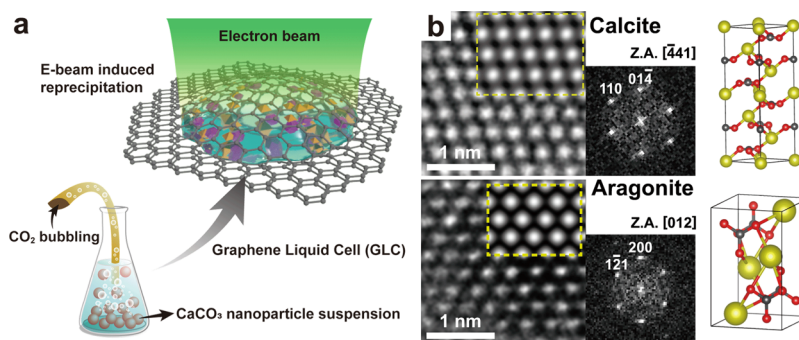


Figure 1. (a) Schematic of the GLC structure containing the calcium bicarbonate solution. The precursor solution is prepared by bubbling carbon dioxide gas into the calcite-suspended water. The precursor solution is then trapped with multilayer graphene membranes. When the GLC was exposed to the electron beam, particles are precipitated as water evaporates. (b) Filtered HRTEM images of the precipitates and the corresponding FFTs with each crystal structure of calcite and aragonite. Simulated images are presented in each of the HRTEM images, surrounded by the dotted yellow line. Z.A. is the zone axis.

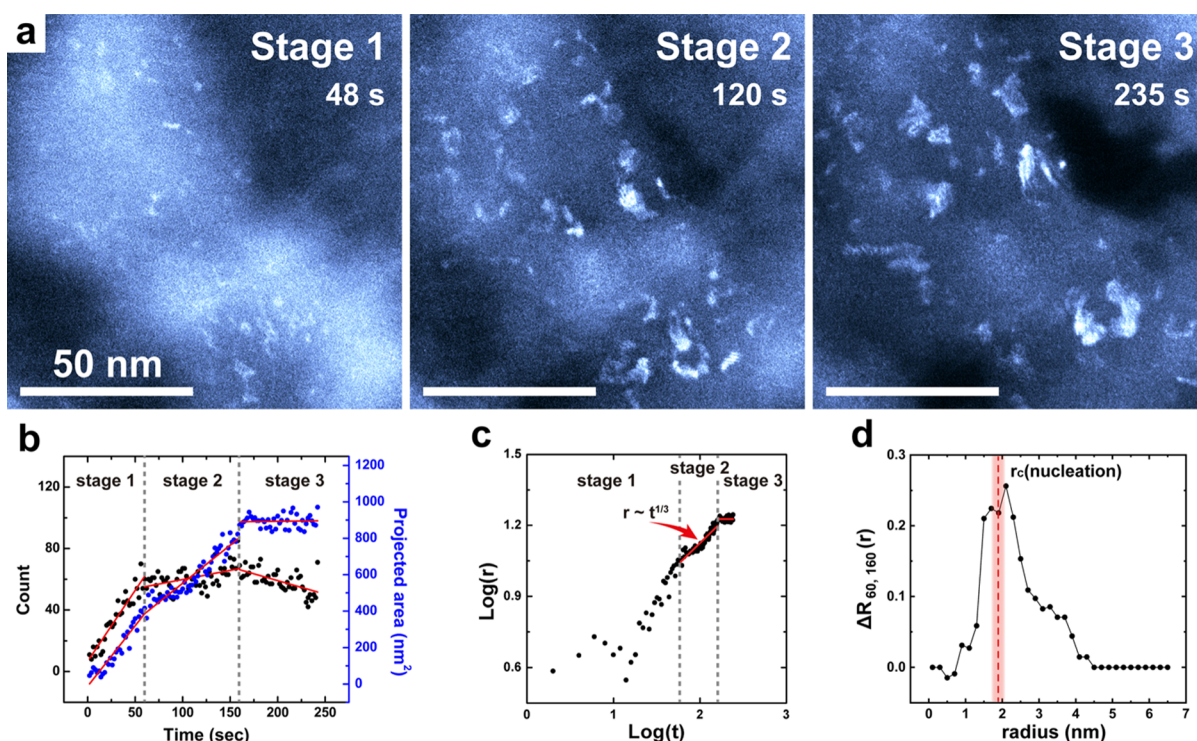


Figure 2. *In situ* dark-field TEM analysis of CaCO_3 crystallization. (a) Time series images corresponding to each mineralization stage. (b) Each black and blue dot gives the number of particles and total projected area of all precipitates as a function of irradiation time t . Based on the dynamics of mineralization, the whole process is divided into three stages: nucleation, diffusion-limited growth, and Ostwald ripening/coalescence. Red solid lines show the trends in each stage. (c) Logarithm relationship between the radius r of the particles and t . (d) Increase in the ratio of the number of particles larger than r during the growth step (Stage 2), $\Delta R_{60,160}(r)$. The peak indicated by the red dotted line shows the critical radius for the nucleation, $r_c(\text{nucleation})$.

graphene membrane that are formed during the wet transfer process.^{22,23} Calcium carbonate particles are nucleated because of the significant changes in the saturation level, followed by nanoparticle growth with further irradiation from the electron beam. At 240 s, the growth of particles eventually stops as the ion species are completely exhausted. The precipitation process in Figure 2a is quantitatively analyzed in Figure 2b–d. The graphs in Figure 2b show the number of particles and their total projection areas as a function of irradiation time t . The number of particles increases dramatically until 60 s, indicating that the initial precipitation process is mainly governed by the nucleation process that is attributed to the supersaturated conditions (Stage 1).²⁴ After 60 s, the growth

rate of the amount of precipitate decreases substantially until 160 s, whereas the growth rate of the total area remains similar to that in the nucleation step. These results indicate that the mineralization process transfers to the growth step from the nucleation step (Stage 2). From 160 s, the amount of precipitate slightly decreases while maintaining the total area, which is explained by Ostwald ripening and coalescence (Stage 3) (Figure S4). Here, the suggested stages are categorized by the overall growth kinetics based on Figure 2b, indicating that the crystallization behavior of the individual particles can differ slightly from the suggested stages. In Figure 2c, a plot of the logarithmic relationship between the particle radius and irradiation time demonstrates that the radii of the precipitates

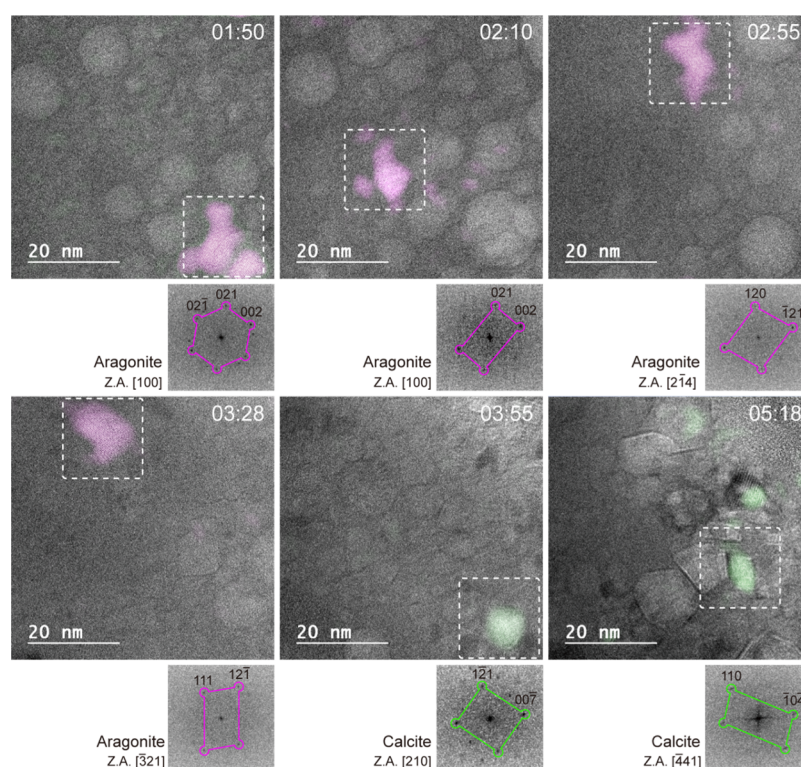


Figure 3. Time series HRTEM images of mineralization are acquired. Nanocrystals are color-coded using IFFTs, where magenta and green represent aragonite and calcite polymorphs, respectively. FFT patterns from the white dotted box are indexed below the corresponding image. The sequential growth of CaCO_3 polymorphs, from aragonite to calcite, shows that the mineralization follows Ostwald's rule of stages. (Z.A. is the zone axis.)

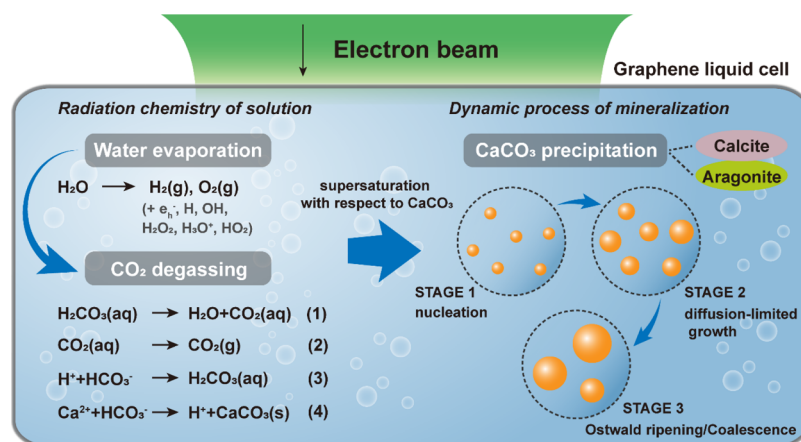


Figure 4. Schematic describing the whole mineralization process in the GLC. Calcium carbonate minerals are precipitated in the highly supersaturated solution by the evaporation of water and the degassing of carbon dioxide. The mineralization process occurs in three distinct stages. Under the highly supersaturated conditions, mineralization of the metastable aragonite phase is preceded by the stable calcite phase.

increase proportionally to $t^{1/3}$ in the second stage, suggesting that the growth is limited primarily by the diffusion process.²⁵ The concentration of the precursor species near the particles is reduced significantly in the nucleation step, resulting in the diffusion-limited growth process within Stage 2.

To determine the critical radius for further stable growth, we introduce an experimental calculation method based on the fundamental definition of the critical radius (see the [Experimental Section](#)). The critical radius for the transition from nucleation to diffusion-limited growth is determined ([Figure 2d](#)) from the variation in the particle size distribution over time. The introduced index, $\Delta R_{t_1, t_2}(r)$, the increase in the

ratio of the number of particles larger than the radius r from t_1 to t_2 , is locally maximized at the critical radius. During the growth step in Stage 2 (from 60 to 160 s), particles larger than the critical radius continue to grow, meaning that $\Delta R_{60, 160}(r)$ is locally maximized as the r approaches the critical radius of the nuclei, $r_c(\text{nucleation})$. Therefore, the peak indicated by the red dotted line corresponds to the $r_c = 1.9$ nm. From the calculated r_c value, we can obtain the average supersaturation level of the solution of 8.54–9.25, based on classical nucleation theory (see [Experimental Section](#)).

In situ HRTEM is conducted ([Figure 3](#) and [Movie S2](#)) to analyze the crystallization of the polymorphs observed in

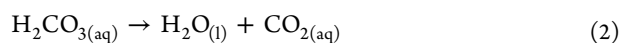
Figure 1b. An inverse fast Fourier transform (IFFT) is used to clarify the polymorphs in the series of images (Figure S5). Nanocrystals, nucleated from 40 s, correspond to the metastable polymorph of aragonite (magenta). The aragonite particles nucleate continuously until 3 min 30 s. Sequentially, the most stable phase of the calcite precipitates from 3 min 38 s (green). Nucleation from aragonite to calcite is clearly identified here, which is ordered by their nucleation barriers and surface energies.²⁶ Therefore, the mineralization of CaCO₃ follows Ostwald's rule of stages, describing that the crystallization of the thermodynamically stable phase is preceded by the formation of metastable polymorphs. Open questions remain regarding the appearance of the amorphous phase, which is a key precursor of crystalline polymorphs. Several *in situ* TEM studies suggest that the amorphous phase is directly transformed into nanocrystals.^{19,27} However, the spatial resolution of the experiments does not allow us to clarify the existence of the amorphous calcium carbonate phase at the initiation of nanocrystal formation.

Figure 4 shows the schematics representing the proposed mineralization mechanism under electron beam irradiation as the following sequential reactions.

Initially, calcium and bicarbonate hydrated solutions are prepared by the Kitano method. Carbonic acid and aqueous carbon dioxide are also present in the solution.



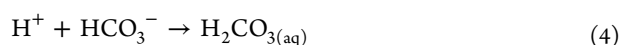
Upon electron beam irradiation, the incident electrons interact with and decompose the water molecules. The decomposition products (e_h^- , H^\bullet , H_2 , H_2O_2 , H_3O^+ , and HO_2^\bullet) interact with the pre-existing aqueous CO₂ and HCO₃⁻ ions, leading to the formation of large amounts of H₂ and O₂ gases (reaction 1).²⁸



Water depletion drives the carbonic acid consumption reaction (reaction 2).



The formation of carbon dioxide gas is promoted by the increasing concentration of aqueous carbon dioxide (reaction 3).



Finally, reactions 4 and 5 must also proceed, ultimately leading to the nucleation of calcium carbonate minerals. In other words, the nucleation of calcium carbonate is ascribed to the increased degree of saturation of the solution and the subsequent deteriorated stability of the ions. Further irradiation promotes the growth of crystals, composed of three stages: nucleation, diffusion-limited growth, and Ostwald ripening/coalescence. Our findings show that CaCO₃ minerals sequentially nucleate from aragonite to calcite, which is consistent with Ostwald's rule of stages. Moreover, under highly supersaturated conditions, the metastable aragonite phase is stabilized with calcite until the cessation of growth (Figure 1b).

3. CONCLUSIONS

In conclusion, GLC-TEM enables us to demonstrate the mineralization dynamics and polymorphs of calcium carbonate with low mass–thickness contrast in TEM. Utilizing *in situ* HRTEM analysis, we observe in real-time that the calcite polymorph grows sequentially after the metastable form of aragonite and verify that the aragonite finally precipitates under the highly supersaturated conditions along with the calcite in the GLC. These results describe the approaches for the selective growth of polymorphs with the control of supersaturation. In addition, we demonstrate that the mineralization process has three stages: nucleation, diffusion-limited growth, and Ostwald ripening/coalescence. This work implies that the GLC allows us to visualize the mineralization process at an atomic scale and hence promises the potential to extend into areas of low mass–thickness contrast materials such as polymers and biogenic substances.

4. EXPERIMENTAL SECTION

4.1. GLC Preparation. Few-layer graphene membranes were synthesized using thermal chemical vapor deposition based on a previous work²⁹ and transferred onto a QUANTIFOIL holey-carbon TEM grid (Ted Pella, Inc.). The Kitano method was applied to the preparation of the precursor solution as follows.³⁰ Initially, CO₂ gas was bubbled through a 5 mM suspended CaCO₃ solution for 24 h. The solution was then filtered with a syringe filter and CO₂ was bubbled again for another 2 h to dissolve the remaining nanoparticles. The GLC was fabricated by enclosing the prepared solution with few-layer graphene sheets. The graphene membranes separated the liquid specimen from the vacuum environment. An incident electron beam was used for TEM imaging to initiate the water evaporation. This method enabled us to control the dynamics without affecting other variables, such as pressure or temperature.

4.2. Pristine Particle Synthesis. Pure calcite particles were used as a pristine material, and the *ex situ* experiment was carried out with the same precursor solution to investigate the effect of dynamics on the polymorph precipitation. The pristine nanoparticles were synthesized by the direct mixing method and characterized *via* TEM analysis and Raman spectroscopy (Figure S6).³¹ The sizes of the synthesized particles were approximately a few tens of nanometers (Figure S6a), aiding in the preparation of a completely dissolved calcium bicarbonate solution during the CO₂ bubbling process.

4.3. In Situ TEM. We used a Tecnai G² F30 S-TWIN for real-time observations of the CaCO₃ mineralization process. The accelerating voltage of the microscope was 80 keV, which has the favorable electron energy for the observation of low mass–thickness materials with an electron dosage of 50 e⁻/Å²·s in dark-field imaging and 837 e⁻/Å²·s in high-resolution imaging conditions. Dark-field images were obtained by positioning the objective aperture on the d-spacing of 2.07, 2.43, and 2.94 Å, corresponding to the calcite and aragonite polymorphs (Figure S3). The liquid contrast was observed simultaneously with the precipitates because the diffuse scattered diffraction from the solution was included in the aperture.

To track the time-sequential changes in the particle growth, the following methods were used. First, time series images were extracted every 2 s from the video (Movie S1). Second, the particles were identified by subtracting the Gaussian

blurred image from the original image. Third, the edges of the particles were drawn. Finally, the number of particles and the projected area were calculated using the plugin of ImageJ software "Analyze Particles".

4.4. Critical Radius Calculation. The calculation of the critical radius, r_c , of the nucleation is based on the definition of the critical radius, which indicates that particles with radii smaller than the r_c would decay and those with greater radii than r_c would grow further. This means that the increase in the ratio of the number of particles larger than radius r over time would be locally maximized at r_c and approach 0 as r moves away from r_c . Therefore, to determine r_c , we introduce the ratio increment index as follows

$$\Delta R_{t_1, t_2}(r) = \left(\sum_{r'_2=r}^{r'_2=r_{\max}} n_{r'_2} / \sum_{r'_2=0}^{r'_2=r_{\max}} n_{r'_2} \right) - \left(\sum_{r'_1=r}^{r'_1=r_{\max}} n_{r'_1} / \sum_{r'_1=0}^{r'_1=r_{\max}} n_{r'_1} \right)$$

where $\Delta R_{t_1, t_2}(r)$ is the increase in the ratio of the number of particles larger than r between times t_1 and t_2 , r_t is the radius of a particle at time point t , n_{r_t} is the number of particles with radius r_t . Therefore, the critical radius can be determined by the local maximum of the $\Delta R_{t_1, t_2}(r)$.

4.5. Supersaturation Calculation. The degree of supersaturation was calculated using classical nucleation theory, which correlates the critical radius for the growth of the nuclei with the supersaturation of the solution

$$r_{\text{crit}} = \frac{2\gamma V_m}{RT \ln S}, \quad S = \exp\left(\frac{2\gamma V_m}{RT r_{\text{crit}}}\right)$$

where r_{crit} is the critical radius that corresponds to the minimum size at which a particle can survive in solution without being dissolved, γ is the interfacial energy of the particle (calcite: $142 \times 10^{-3} \text{ N}\cdot\text{m}^{-1}$, aragonite: $149 \times 10^{-3} \text{ N}\cdot\text{m}^{-1}$), V_m is the molar volume of a particle (calcite: $3.69 \times 10^{-5} \text{ m}^3\cdot\text{mol}^{-1}$, aragonite: $3.39 \times 10^{-5} \text{ m}^3\cdot\text{mol}^{-1}$), R is the universal gas constant, T is the temperature, and S is the supersaturation of the solution.^{32,33}

■ ASSOCIATED CONTENT

SI Supporting Information

The Supporting Information is available free of charge at <https://pubs.acs.org/doi/10.1021/acsomega.0c01300>.

Low-magnification bright-field TEM images of GLCs; raw HRTEM images of calcite and aragonite; imaging conditions for DF-TEM; Ostwald ripening and coalescence of the particles; image processing procedure using IFFTs; bright-field TEM image, diffraction pattern, high-resolution TEM image, and Raman spectrum from pristine calcite nanoparticles; calcination of the calcite and CaO by electron beam radiolysis; SEM image and Raman spectrum of *ex situ*-precipitated calcium carbonate minerals under ambient conditions (PDF)

In situ DF-TEM movie for CaCO₃ mineralization and *in situ* HRTEM movie for CaCO₃ mineralization (MP4)

(MP4)

■ AUTHOR INFORMATION

Corresponding Author

Jong Min Yuk – Department of Materials Science and Engineering, Korea Advanced Institute of Science and Technology, Daejeon 305-701, Republic of Korea; orcid.org/0000-0002-4677-7363; Email: jongmin.yuk@kaist.ac.kr

Authors

Kyun Seong Dae – Department of Materials Science and Engineering, Korea Advanced Institute of Science and Technology, Daejeon 305-701, Republic of Korea; orcid.org/0000-0001-5928-9855

Joon Ha Chang – Department of Materials Science and Engineering, Korea Advanced Institute of Science and Technology, Daejeon 305-701, Republic of Korea; orcid.org/0000-0001-8877-9917

Kunmo Koo – Department of Materials Science and Engineering, Korea Advanced Institute of Science and Technology, Daejeon 305-701, Republic of Korea; orcid.org/0000-0003-3031-5903

Jungjae Park – Department of Materials Science and Engineering, Korea Advanced Institute of Science and Technology, Daejeon 305-701, Republic of Korea

Jae Sung Kim – Department of Materials Science and Engineering, Korea Advanced Institute of Science and Technology, Daejeon 305-701, Republic of Korea

Complete contact information is available at: <https://pubs.acs.org/10.1021/acsomega.0c01300>

Notes

The authors declare no competing financial interest.

■ ACKNOWLEDGMENTS

This work was supported by the Nano-Material Technology Development Program through the National Research Foundation of Korea (NRF) funded by the Ministry of Science, ICT and Future Planning (2009-0082580), and NRF grant funded by the Korea government (MSIP; Ministry of Science, ICT & Future Planning) (NRF-2018R1C1B6002624).

■ REFERENCES

- (1) Blatt, H.; Tracy, R.; Owens, B. *Petrology: Igneous, Sedimentary, and Metamorphic*, 3rd ed.; W. H. Freeman & Company: New York, 2006.
- (2) Bathurst, R. G. C. *Carbonate Sediments and Their Diagenesis*, 1st ed.; Elsevier: New York, 1972.
- (3) Hill, C.; Forti, P. *Cave Minerals of the World*, 2nd ed.; National Speleological Society: Huntsville, Alabama, 1997; pp 285–287.
- (4) Railsback, L. B.; Brook, G. A.; Chen, J.; Kalin, R.; Fleisher, C. J. Environmental Controls on the Petrology of a Late Holocene Speleothem from Botswana with Annual Layers of Aragonite and Calcite. *J. Sediment. Res., Sect. A* **1994**, *64*, 147–155.
- (5) Nancollas, G. H.; Reddy, M. M. Kinetics of Crystallization of Scale-Forming Minerals. *Soc. Pet. Eng. J.* **1974**, *14*, 117–126.
- (6) Engel, J. A *Critical Survey of Biomineralization*; Springer: New York, 2016.
- (7) Lowenstam, H. A.; Weiner, S. *On Biomineralization*; Oxford University Press: New York, 1989.
- (8) Morse, J. W.; Arvidson, R. S.; Lüttge, A. Calcium carbonate formation and dissolution. *Chem. Rev.* **2007**, *107*, 342–381.
- (9) Reeder, R. J. *Carbonates: Mineralogy and Chemistry*; De Gruyter: Washington, DC, 1983; Vol. 11.

- (10) Kim, W.-S.; Hirasawa, I.; Kim, W.-S. Polymorphic change of calcium carbonate during reaction crystallization in a batch reactor. *Ind. Eng. Chem. Res.* **2004**, *43*, 2650–2657.
- (11) Hu, Z.; Deng, Y. Supersaturation control in aragonite synthesis using sparingly soluble calcium sulfate as reactants. *J. Colloid Interface Sci.* **2003**, *266*, 359–365.
- (12) Vagenas, N.; Gatsouli, A.; Kontoyannis, C. G. Quantitative analysis of synthetic calcium carbonate polymorphs using FT-IR spectroscopy. *Talanta* **2003**, *59*, 831–836.
- (13) Qiao, Z.; Liu, X.; Duan, X.; Zhou, Y.; Pei, C.; Ma, Y. Biomimetic interfacial assembly of CaCO₃ microspheres using egg-white foam and their interaction with Sr²⁺. *Ceram. Int.* **2017**, *43*, 12870–12875.
- (14) Butto, N.; Cabrera-Barjas, G.; Neira-Carrillo, A. Electro-crystallization of CaCO₃ crystals obtained through phosphorylated chitin. *Crystals* **2018**, *8*, 82.
- (15) Chen, J.; Jiang, M.; Su, M.; Han, J.; Li, S.; Wu, Q. Mineralization of calcium carbonate induced by egg substrate and an electric field. *Chem. Eng. Technol.* **2019**, *42*, 1525–1532.
- (16) Smeets, P. J. M.; Cho, K. R.; Kempen, R. G. E.; Sommerdijk, N. A. J. M.; De Yoreo, J. J. Calcium carbonate nucleation driven by ion binding in a biomimetic matrix revealed by in situ electron microscopy. *Nat. Mater.* **2015**, *14*, 394–399.
- (17) Nielsen, M. H.; Aloni, S.; De Yoreo, J. J. In situ TEM imaging of CaCO₃ nucleation reveals coexistence of direct and indirect pathways. *Science* **2014**, *345*, 1158–1162.
- (18) Stawski, T. M.; Roncal-Herrero, T.; Fernandez-Martinez, A.; Matamoros-Veloza, A.; Kröger, R.; Benning, L. G. “On demand” triggered crystallization of CaCO₃ from solute precursor species stabilized by the water-in-oil microemulsion. *Phys. Chem. Chem. Phys.* **2018**, *20*, 13825–13835.
- (19) Liu, Z.; Zhang, Z.; Wang, Z.; Jin, B.; Li, D.; Tao, J.; Tang, R.; De Yoreo, J. J. Shape-preserving amorphous-to-crystalline transformation of CaCO₃ revealed by in situ TEM. *Proc. Natl. Acad. Sci. U.S.A.* **2020**, *117*, 3397–3404.
- (20) Yuk, J. M.; Zhou, Q.; Chang, J.; Ercius, P.; Alivisatos, A. P.; Zettl, A. Real-time observation of water-soluble mineral precipitation in aqueous solution by in situ high-resolution electron microscopy. *ACS Nano* **2016**, *10*, 88–92.
- (21) Pobeguain, T. Sur les concrétions calcaires Observées dans la Grotte de Moulis (Ariège). *C. R. Seances Acad. Sci., Ser. B* **1955**, *241*, 1791–1793.
- (22) Hauwiller, M. R.; Ondry, J. C.; Alivisatos, A. P. Using graphene liquid cell transmission electron microscopy to study in situ nanocrystal etching. *J. Visualized Exp.* **2018**, *135*, No. e57665.
- (23) Kim, Q.; Shin, D.; Park, J.; Weitz, D. A.; Jhe, W. Initial growth dynamics of 10 nm nanobubbles in the graphene liquid cell. *Appl. Nanosci.* **2018**, 1–7.
- (24) Bahrig, L.; Hickey, S. G.; Eychmüller, A. Mesocrystalline materials and the involvement of oriented attachment - a review. *CrystEngComm* **2014**, *16*, 9408–9424.
- (25) Ham, F. S. Theory of diffusion-limited precipitation. *J. Phys. Chem. Solids.* **1958**, *6*, 335–351.
- (26) Sun, W.; Jayaraman, S.; Chen, W.; Persson, K. A.; Ceder, G. Nucleation of metastable aragonite CaCO₃ in seawater. *Proc. Natl. Acad. Sci. U.S.A.* **2015**, *112*, 3199–3204.
- (27) Yang, J.; Koo, J.; Kim, S.; Jeon, S.; Choi, B. K.; Kwon, S.; Kim, J.; Kim, B. H.; Lee, W. C.; Lee, W. B.; Lee, H.; Hyeon, T.; Ercius, P.; Park, J. Amorphous-phase-mediated crystallization of Ni nanocrystals revealed by high-resolution liquid-phase electron microscopy. *J. Am. Chem. Soc.* **2019**, *141*, 763–768.
- (28) Schneider, N. M.; Norton, M. M.; Mendel, B. J.; Grogan, J. M.; Ross, F. M.; Bau, H. H. Electron-water interactions and implications for liquid cell electron microscopy. *J. Phys. Chem. C* **2014**, *118*, 22373–22382.
- (29) Tu, Z.; Liu, Z.; Li, Y.; Yang, F.; Zhang, L.; Zhao, Z.; Xu, C.; Wu, S.; Liu, H.; Yang, H.; Richard, P. Controllable growth of 1-7 layers of graphene by chemical vapour deposition. *Carbon* **2014**, *73*, 252–258.
- (30) Kitano, Y. A study of the polymorphic formation of calcium carbonate in thermal springs with an emphasis on the effect of temperature. *Bull. Chem. Soc. Jpn.* **1962**, *35*, 1980–1985.
- (31) Babou-Kammoe, R.; Hamoudi, S.; Larachi, F.; Belkacemi, K. Synthesis of CaCO₃ nanoparticles by controlled precipitation of saturated carbonate and calcium nitrate aqueous solutions. *Can. J. Chem. Eng.* **2012**, *90*, 26–33.
- (32) Donnet, M.; Bowen, P.; Lemaître, J. A thermodynamic solution model for calcium carbonate: Towards an understanding of multi-equilibria precipitation pathways. *J. Colloid Interface Sci.* **2009**, *340*, 218–224.
- (33) MacDonald, G. J. Experimental determination of calcite-aragonite equilibrium relations at elevated temperatures and pressures. *Am. Mineral.* **1956**, *41*, 744–756.